

## Research Article

Swimmer with submerged SiO<sub>2</sub>/Al/LiNbO<sub>3</sub> surface acoustic wave propulsion systemDeqing Kong<sup>a,\*</sup>, Ryo Tanimura<sup>a</sup>, Fang Wang<sup>b</sup>, Kailiang Zhang<sup>b</sup>, Minoru Kuribayashi Kurosawa<sup>c</sup>, Manabu Aoyagi<sup>a</sup><sup>a</sup> Department of Engineering, Muroran Institute of Technology, Muroran 050-8585, Japan<sup>b</sup> Tianjin Key Laboratory of Film Electronic and Communication Devices, School of Integrated Circuit Science and Engineering, Tianjin University of Technology, Tianjin 300384, China<sup>c</sup> School of Engineering, Tokyo Institute of Technology, Yokohama 226-8501, Japan

## ARTICLE INFO

## Article history:

Received 21 January 2024

Revised 3 March 2024

Accepted 3 April 2024

Available online 6 April 2024

## Keywords:

Acoustofluidics

Surface acoustic wave

Swimmer

Underwater propulsion system

## ABSTRACT

Acoustic propulsion system presents a novel underwater propulsion approach in small scale swimmer. This study introduces a submerged surface acoustic wave (SAW) propulsion system based on the SiO<sub>2</sub>/Al/LiNbO<sub>3</sub> structure. At 19.25 MHz, the SAW propulsion system is proposed and investigated by the propulsion force calculation, PIV measurements and propulsion measurements. 3.3 mN propulsion force is measured at 27.6 V<sub>pp</sub>. To evaluate the miniature swimmer, the SAW propulsion systems with multiple frequencies are studied. At 2.2 W, the submerged SAW propulsion system at 38.45 MHz demonstrates 0.83 mN/mm<sup>2</sup> propulsion characteristics. At 96.13 MHz and 24 V<sub>pp</sub>, the movements of miniature swimmer with a fully submerged SAW propulsion system are recorded and analyzed to a maximum of 177 mm/s. Because of miniaturization, high power density, and simple structure, the SAW propulsion system can be expected for some microrobot applications, such as underwater drone, pipeline robot and intravascular robot.

© 2024 The Author(s). Published by Elsevier B.V. on behalf of Shandong University. This is an open access article under the CC BY license (<http://creativecommons.org/licenses/by/4.0/>).

## 1. Introduction

Mechanical structures convert energy into actuation in water for swimmers, such as the screw, tail and others [1–3]. In the field of underwater propulsion systems, the propeller, bionic fin and jet system can be summed up as mechanical principles. Propellers and jet systems are widely applied in ships and underwater robots because of their powerful propulsion force. They play a significant role in transportation and exploration. Fish-shaped underwater robots have also been reported [1]. On the other hand, magnetic, acoustic and biochemical propulsion systems have been studied widely in micro-environments [4–8]. Based on the external magnetic and acoustic system, microrobots can be manipulated and moved to a specified position in the liquid environments [9–11]. Some tiny swimmers rely on chemical power that converts local fuels to drive their motion [12,13]. The fundamental principles of these swimmers, with rich chemistry, have been studied for biomedical applications. The characteristics of miniaturization allow them to be competent for more delicate tasks, such as cell drug delivery systems and minimally invasive surgery [14–17]. Underwater propulsion methods are summarized in Table 1. Despite widespread applications of propulsion

systems in various fields, there are still major technical problems and challenges. Typically the coexistence of high thrust and miniaturization is an inescapable issue.

In the field of acoustofluidic technologies, acoustic driving force within fluids has been utilized to manipulate fluids and particles in a noncontact and biocompatible manner [18–22]. Acoustic streaming force and acoustic radiation force, is the representative of acoustic driving force, are discussed and applied in medical and biological devices [23–28]. Recently, acoustic propulsion force (APS), which is the reaction force of the acoustic driving force, as a new scheme to realize the autonomous locomotion of swimmer. A novel acoustic propulsion system is introduced to try to explore high output power and miniaturization with surface acoustic waves (SAW) and bulk acoustic waves (BAW) in Table 1 [29–33]. In this nonlinear phenomenon, the outstanding mechanical properties of fluids make them anticipated as a novel type of underwater propulsion system. In the new area of acoustofluidic actuation application, the SAW propulsion system is proposed and investigated because of miniaturization with high frequency. In this work, a submerged interdigital transducer (IDT) based on SiO<sub>2</sub>/Al/LiNbO<sub>3</sub> structure is designed and studied for miniaturization and high-power density. IDT submergence leads to a higher acoustic propulsion efficiency in water. A SiO<sub>2</sub> film is coated on the surface of IDT as an insulating layer. The propulsion force characteristics, frequency characteristics and swimmer

\* Corresponding author.

E-mail addresses: [kong@muroran-it.ac.jp](mailto:kong@muroran-it.ac.jp), [kong@toyota-ti.ac.jp](mailto:kong@toyota-ti.ac.jp) (D. Kong).

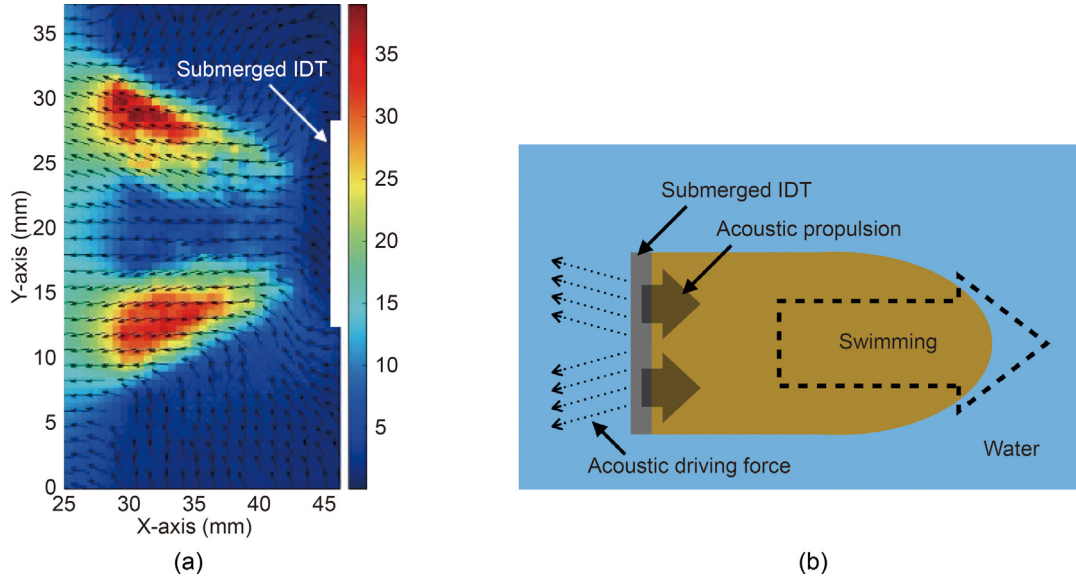


**Fig. 1.** SAW propulsion principle with submerged IDT. (a) Flow velocity distribution at 9.61 MHz and 27.6  $V_{pp}$ . (b) Schematic diagram of prototype swimmer with IDT.

**Table 1**  
Underwater propulsion methods for swimmer.

| Method                                     | Advantages  | Disadvantages                                     |
|--|---|---|
| Screw                                      | High propulsion force                                     | Complicated structure                             |
| Tail                                       | Low fluid resistance                                      | Complicated structure                             |
| External magnetic propulsion               | Simple structure<br>Miniaturization                       | Low propulsion force<br>External magnetic control |
| External acoustic propulsion               | Simple structure<br>Miniaturization                       | Low propulsion force<br>External acoustic control |
| Biochemical propulsion                     | Simple structure<br>Miniaturization                       | Low propulsion force                              |
| Acoustic autonomous propulsion (This work) | Simple structure<br>Miniaturization<br>High power density | Need more investigation                           |

movement based on  $\text{SiO}_2/\text{Al}/\text{LiNbO}_3$  SAW propulsion system are reported and evaluated. The fully submerged SAW propulsion system is more suitable as a small-scale and high-power propulsion system. Thus, a SAW propulsion system with submerged IDT makes such systems suitable for applications such as underwater drone, pipeline inspection robot and intravascular robot in future.

## 2. Surface acoustic wave acoustofluidics for autonomous propulsion system

In the area of acoustofluidic actuation, manipulation, micropump and atomization have been studied and applied for a long time [20–28]. Acoustofluidic actuation utilizes acoustic waves to manipulate fluids and particles within fluids and has new applications, such as the drug delivery system, cell therapy, and pharmaceuticals. In the case of acoustic driving force (ADF) in liquid, the particle manipulation can be characterized by acoustic radiation force (ARF) and acoustic streaming force (ASF) with the SAW device. Underwater SAW propulsion system utilizes acoustic waves to achieve an autonomous movement in novel areas of acoustofluidic actuation. When the IDT as a propulsion source is placed freely in water, swimmers with acoustic propulsion systems realize the self-motion [34–36]. In terms of bio-inspired and biomimetic engineering, the high pressure in the vibration surface acts to push fluid downstream, propelling the swimmer forward as a consequence [36,37]. As shown in Fig. 1(a), the flow

velocity distribution is observed with particle image velocimetry (PIV) measurement at 9.61 MHz and 27.6  $V_{pp}$ , when the IDT is set in whole submergence. Longitudinal waves are generated into the water with the Rayleigh angle of  $\theta_R$  ( $\theta_R = \sin^{-1}c_1/c_2$ ,  $c_1$ : phase velocity of the longitudinal wave,  $c_2$ : propagation velocity of Rayleigh wave). Thus, the submerged IDT can be as a propulsion source in water in Fig. 1(b). When ADF is generated by the submerged IDT, swimmer with the SAW propulsion system can swim in the opposite direction.

The SAW is an elastic wave propagating along the free surface. When the surface of the substrate is sunk into the liquid, a leaky surface acoustic wave (LSAW), converted from Rayleigh surface acoustic wave (RSAW), propagates along the boundary surface between the solid and liquid. In this nonlinear acoustic phenomenon, acoustic propulsion, that is the reaction force of the ADF, can be evaluated and investigated with ARF in the boundary surface between the solid transducer and liquid. Acoustic radiation pressure (ARP)  $P$ , or the discrepancies in fluid energy density due to LSAW [38–40], can be calculated as

$$P = \frac{1}{2}\rho v^2 + \frac{1}{2}\frac{c_1^2}{\rho}\rho'^2 \quad (1)$$

where  $\rho$  is the liquid density and  $v$  is the particle velocity.  $c_1$  is the phase velocity of the longitudinal wave in liquid, and  $\rho'$  is the liquid density fluctuation. When the traveling wave is generated into the liquid, ARP in Eq. (1) can be represented by

$$P = \rho v^2 \quad (2)$$

In the case of LSAW, the displacements of  $u_x$  and  $u_z$  in LSAW propagation direction  $x$ -axis and normal direction  $z$ -axis in the boundary surface between solid transducer and liquid can be expressed as

$$u_x = Ae^{j\omega t} e^{-jk_L x} e^{-\alpha k_L z} \quad (3)$$

$$u_z = -j\alpha Ae^{j\omega t} e^{-jk_L x} e^{-\alpha k_L z} \quad (4)$$

where  $A$ ,  $\omega$  and  $k_L$  are the normal vibration amplitude, angular frequency and wave number, respectively. Absorption coefficient  $\alpha$  can be calculated as

$$\alpha = \sqrt{1 - \frac{c_2^2}{c_1^2}} \quad (5)$$

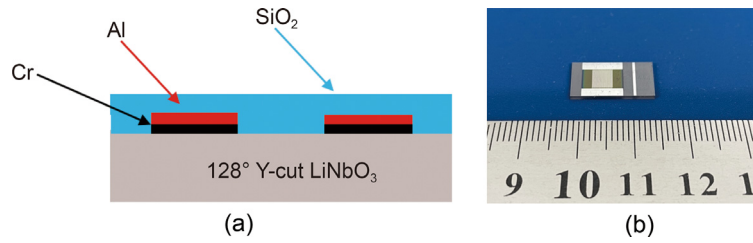


Fig. 2. IDT at 19.25 MHz. (a) Schematic cross-section structure of SiO<sub>2</sub>/Al/LiNbO<sub>3</sub> SAW propulsion system. (b) Photograph of IDT.

Table 2

Parameters of IDT at 19.25 MHz.

| Parameters            | IDT |
|-----------------------|-----|
| Periodic length (μm)  | 200 |
| Aperture (mm)         | 4.5 |
| Strip-electrode pairs | 20  |
| Metallization ratio   | 0.5 |

where  $c_2$  is the propagation velocity of Rayleigh wave in solid. Particle velocity  $v$  is calculated using Eqs. (3) and (4). ARP in Eq. (2) can be represented by

$$P = \frac{1}{2} \rho (1 + \alpha^2) v_0^2 e^{2(k_i x + k_i z)} \quad (6)$$

Thus, ARP distribution can be analytically determined using continuous displacement in the boundary surface between solid transducer and liquid. Where  $v_0$  and  $k_i$  are the vibration velocity of the substrate surface and the imaginary part of the LSAW wave number. When  $z = 0$ , ARP can be discussed and investigated in the boundary surface between IDT and liquid.

### 3. IDT at 19 MHz

In previous research, half of the wave power cannot be used as the propulsion force when the IDT is set in edge [34–36], because the SAW is generated with IDT symmetrically in both directions. As shown in Fig. 1(a), Thus, a submerged IDT based on SiO<sub>2</sub>/Al/LiNbO<sub>3</sub> structure is designed and studied for the high-power density and miniaturization [37]. IDT submergence may lead to a higher acoustic propulsion efficiency in water.

#### 3.1. Design

To study the SAW propulsion with submerged IDT, Rayleigh wave was generated in the 128° Y-rotated X-propagation lithium niobate (LiNbO<sub>3</sub>) substrate. At 19.25 MHz, the detail of IDT was shown and determined in Table 2 and Fig. 2(a). The periodic length of IDT was 200 μm, when the driving frequency was 19.25 MHz. The aperture, strip-electrode pairs, and metallization ratio were 4.5 mm, 20, and 0.5. The IDT was fabricated by the surface micro-machining process. Aluminum electrodes were deposited by sputtering deposition in the surface of the substrate. A SiO<sub>2</sub> film was coated on the surface of IDT as an insulating layer. A SiO<sub>2</sub>/Al/LiNbO<sub>3</sub> SAW propulsion system was fabricated in Fig. 2(b).

The admittance characteristics of IDT were measured with an impedance analyzer (IM7580 A, HIOKI) in air and water, respectively. The results were shown in Fig. 3. The resonance frequency was 19.25 MHz in air and water. The conductance of the IDT was 10.5 and 9.9 mS in air and water. The susceptance of the IDT was 3 and 4.7 mS respectively.

To evaluate the vibration characteristics, the normal vibration velocity of SAW at 91 spots was scanned using a laser Doppler

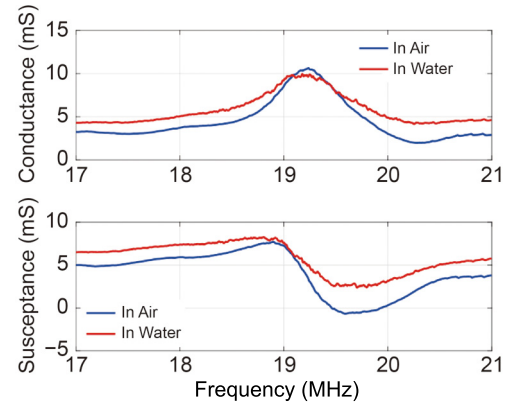


Fig. 3. Admittance characteristics of IDT in air and water: result in air is shown by blue line, result in water is shown by red line.

vibrometer (LDV, Polytec, VibroOne, VIO-130) in the 5 mm aperture range for five different driving voltages in air, as shown in Fig. 4(a). The interval between adjacent spots was 50 μm. Additionally, The average vibration velocity of 91 spot measurements at the different voltages were shown in Fig. 4(b). For an input voltage of 24.8 V<sub>pp</sub>, the average vibration velocity was kept at 0.68 m/s at 19.25 MHz. Thus, high power density nanomechanical vibration of IDT was confirmed.

#### 3.2. Fluid downstream via IDT

The flow velocity was measured using PIV measurement to investigate fluid downstream with the SAW propulsion system at the various input voltages. To study the velocity field, 10-μm seed particles were added to pure deionized water. The measurement area was illuminated with a laser sheet (Civillasers, 530 nm 1.2 W). The flow velocity was recorded with a high-speed camera (FASTCAM Mini UX50, 500 fps). The flow velocity distributions in water at 19.25 MHz were shown in Fig. 5, when the IDT was fully submerged with increasing input voltage. When the IDT was set in whole submergence at 27.6 V<sub>pp</sub>, two fluid streams were generated symmetrically into the water with  $\theta_R$ . The maximum flow velocity in water increased from 34.2 to 86 mm/s when the input voltage was increased from 12.2 to 27.6 V<sub>pp</sub>. Thus, the submerged IDT can be as a propulsion source in water in Fig. 1(b).

#### 3.3. Propulsion characteristics

The acoustic propulsion  $F_{AP}$  is expressed as the reaction force of the ADF. ARP  $P$  is exerted as a type of ADF in the boundary surface of the solid and liquid because of their different acoustic impedances. The vibration velocity in water can be estimated with measured results  $v_m$  in air and the admittance characteristics of IDT in air and water. Since the vibration distribution can be approximated as a sine wave, the average vibration velocity of

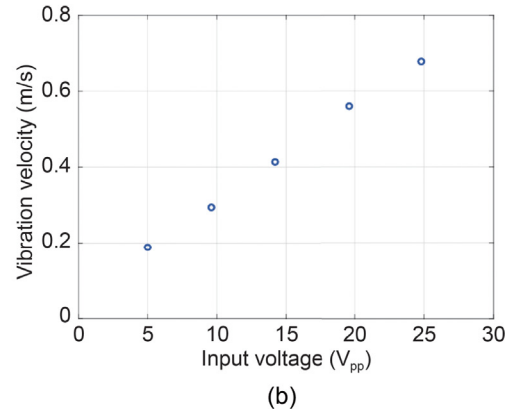
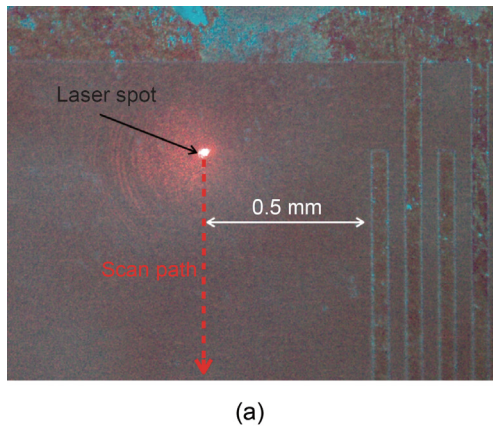


**Fig. 4.** Normal vibration velocity of SAW. (a) Schematic diagram of measurement setup. 91 spots are scanned at 0.5 mm front of IDT. (b) Vibration velocity for various input voltages. At 19.25 MHz and 24.8  $V_{pp}$ , the vibration velocity is 0.68 m/s.

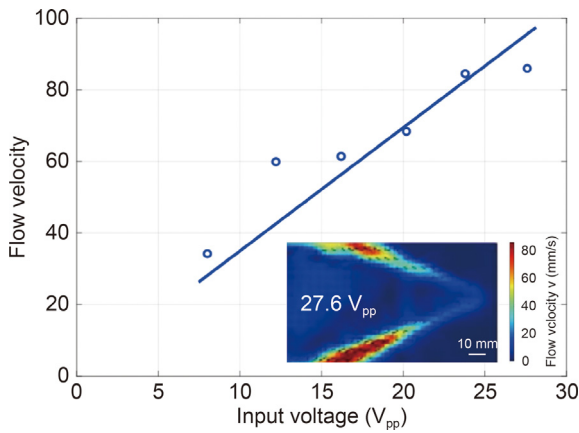


**Fig. 5.** Flow velocity with PIV. Maximum flow velocity increased (from 34.2 to 86 mm/s) with increasing input voltage (from 8 to 27.6  $V_{pp}$ ).

substrate surface  $v_0$  in the propagation direction can be expressed as

$$v_0 = \frac{2}{\pi} v_m \quad (7)$$

When  $\alpha = 0$  in Eq. (6),  $F_{ARF}$  can be calculated with  $v_0$ , vibration area  $S$  and Rayleigh angle of  $\theta_R$  as

$$F_{ARF} = PS\theta_R \quad (8)$$

$S$  can be calculated with the periodic length, aperture and strip-electrode pairs of IDT in Table 2. Thus,  $F_{AP}$  can be represented by

$$F_{AP} = -F_{ARF} \quad (9)$$

To evaluate  $F_{AP}$  for the IDT in water, zero-speed propulsion (ZSP), an important indicator of the SAW propulsion system, was measured using a force gauge (Mark-10, M5-012) in Fig. 6(a). Because the IDT was fixed to the force gauge, the whole SAW propulsion SAW did not move. Thus, the measured results for ZSP forces were difficult to be affected by the fluid resistance, wire traction and other effects, and can be used as a performance indicator for the SAW propulsion system. Fig. 6(b) showed the measured results of ZSP force and  $F_{AP}$  calculation in Eq. (9). The results increased with increasing input voltages. At 27.6  $V_{pp}$ , 3.3 mN ZSP force was measured when the IDT was at a standstill. The distributions of the measured ZSP and calculated  $F_{AP}$  were approximately normal. The measured and calculated

results were around 1.8 and 2.6 mN at 20.2 and 19.6  $V_{pp}$ . The vibration velocity measurements, neglect of viscosity calculation and others may lead to deviations between the measurement and calculation. In future, the calculation result may be improved with the vibration velocity measurement of propagation direction in water and optimized calculation to optimize the propulsion force simulation.

#### 4. Miniaturization via high frequency

The mechanical vibration output power density of SAW is proportional to the surface vibration velocity of IDT in Eq. (6). Because vibration velocity does not greatly change with lower vibration amplitude and higher driving frequency, the ultrasonic actuation with miniature transducer widely discussed and applied [41–47]. Thus, the coexistence of high thrust and miniaturization based on SAW propulsion systems can be expected with the high driving frequency. Advancing the miniaturization of SAW propulsion systems at the microscales thus holds considerable promise for underwater drone, pipeline inspection robot and intravascular robot.

##### 4.1. Frequency characteristics

To evaluate the miniaturization via high frequency, the detail of IDTs at 29.13, 38.45, 48.06, 68.22, 80.2 and 96.13 MHz were determined in Table 3. The metallization ratio was 0.5. IDT areas with  $\text{SiO}_2/\text{Al}/\text{LiNbO}_3$  structure were 8.71, 6, 4, 2.35, 1.73 and 1.2  $\text{mm}^2$ . ZSP measurements of IDTs in water were measured with the force gauge. Fig. 7 showed the measured results of ZSP results with unit area when the input power was 2.2 W. ZSP results fluctuated with different frequencies. At the same input power, IDT at 38.45 MHz demonstrated the most excellent ZSP characteristics. ZSP force per unit area was 0.83  $\text{mN}/\text{mm}^2$ . When the IDT area is reduced to 1.2  $\text{mm}^2$  with increasing driving frequencies, the propulsion force of the miniature SAW propulsion systems also deserves to be expected as an underwater propulsion microsystem.

##### 4.2. Miniature swimmer at 96.13 MHz

In the case of 96.13 MHz and 1.2  $\text{mm}^2$  IDT area, the measured ZSP result was less than 0.1 mN at 2.2 W. To investigate the swimmer locomotion, the no-load speed (NLS) of the swimmer with a 96.13 MHz SAW propulsion system was measured in water. As shown in Fig. 8, a miniature prototype swimmer was

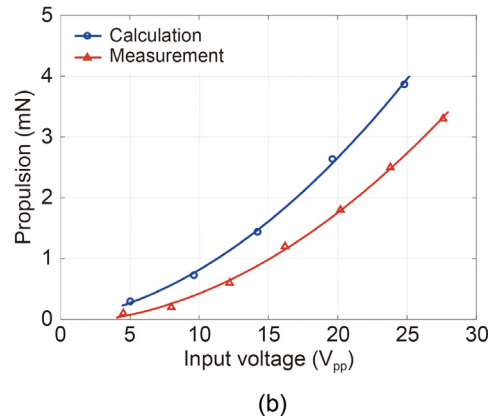
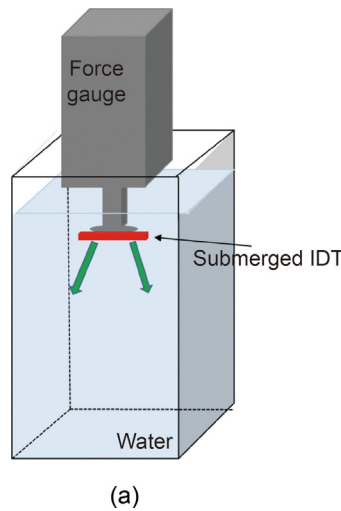


**Fig. 6.** SAW propulsion force. (a) Schematic diagram of measurement setup. (b) The result of acoustic propulsion: calculation (blue) and ZSP measurement (red) for input voltage at 19.25 MHz.

**Table 3**  
Parameters of IDT with different frequencies.

| Frequency (MHz) | Periodic length (μm) | Aperture (mm) | IDT area (mm <sup>2</sup> ) | Strip-electrode pairs | Metallization ratio |
|-----------------|----------------------|---------------|-----------------------------|-----------------------|---------------------|
| 29.13           | 144                  | 3.3           | 8.71                        | 20                    | 0.5                 |
| 38.45           | 100                  | 3             | 6                           |                       |                     |
| 48.06           | 80                   | 2.5           | 4                           |                       |                     |
| 68.22           | 56                   | 2.1           | 2.35                        |                       |                     |
| 80.2            | 48                   | 1.8           | 1.73                        |                       |                     |
| 96.13           | 40                   | 1.5           | 1.2                         |                       |                     |

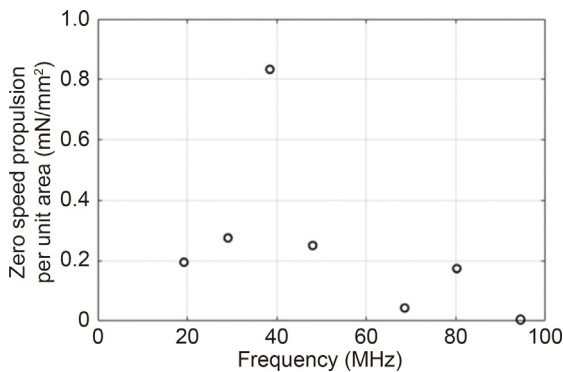


**Fig. 7.** ZSP characteristics per unit area for input voltage at 2.2 W.

designed and fabricated. The dimensions and weight of the prototype swimmer were 10 × 10 × 25 mm and 1 g. A green square acrylonitrile butadiene styrene (ABS) polymer plate was used as an identification mark. A styrofoam kickboard was used to keep balance.

At 24 V<sub>pp</sub>, the locomotion of the prototype swimmer was recorded by a camera in Fig. 9. Based on the green square mark, the recorded video was analyzed using an image recognition program in MATLAB in Fig. 10. The NLS results changeover time in the x and y axis directions was analyzed even though the trajectory of the swimmer was not a perfectly straight line. When the input voltage was applied to the IDT, the NLS result of the prototype swimmer increased to a maximum of 177 mm/s. The speed decreased with fluid resistance and wire traction with the power off. The NLS results for maximum value with increased

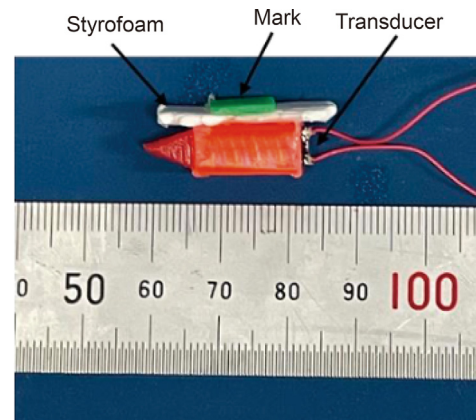


**Fig. 8.** Photograph of acrylic prototype swimmer (10 × 10 × 25 mm).

input voltages were shown in Fig. 11. As the input voltage increased, the maximum NLS results of the prototype swimmer also increased.

## 5. Conclusion

To evaluate the miniaturization and high-power density of the SAW propulsion system, a submerged IDT based on SiO<sub>2</sub>/Al/LiNbO<sub>3</sub> structure was designed and studied. Because the SAW was generated with IDT symmetrically in both directions, the whole IDT submergence made a higher acoustic propulsion efficiency in water. A SiO<sub>2</sub> film was coated on the surface of IDT as an insulating layer. The SAW propulsion system with SiO<sub>2</sub>/Al/LiNbO<sub>3</sub> structure at 19.25 MHz was investigated by the propulsion force calculation, PIV measurements and ZSP results. Based on the admittance characteristics of IDT, fluid downstream and propulsion characteristics, the submerged SAW propulsion system at 19.25 MHz was proposed and discussed. At 27.6 V<sub>pp</sub>, 3.3 mN ZSP force was measured. The distributions of the results of measured ZSP and calculation were approximately normal. On the other hand, to evaluate the miniaturization via high frequency, SAW propulsion systems with IDT at 29.13, 38.45, 48.06, 68.22, 80.2 and 96.13 MHz were evaluated and investigated. At 2.2 W, the submerged SAW propulsion system at 38.45 MHz demonstrated the most

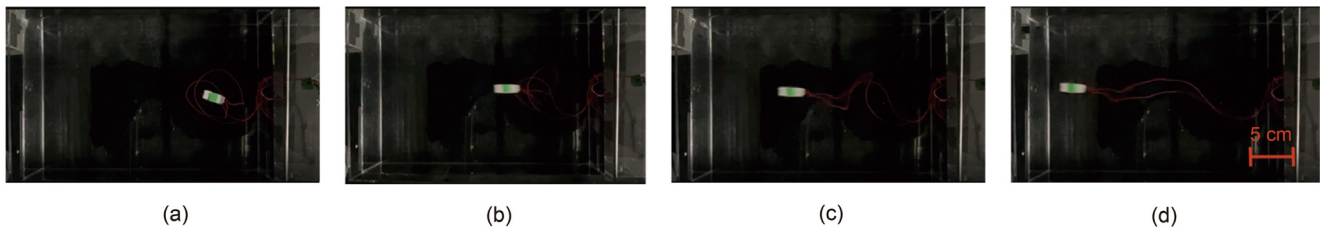


Fig. 9. Swimmer locomotion in water for input voltage of  $24 V_{pp}$  at 96.13 MHz recorded by a camera.

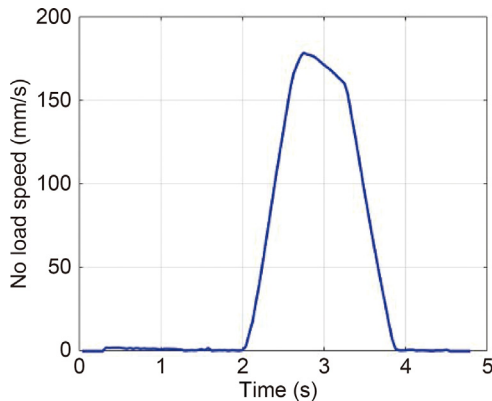


Fig. 10. NLS results for input voltage of  $24 V_{pp}$ . Peak value is 177 mm/s.

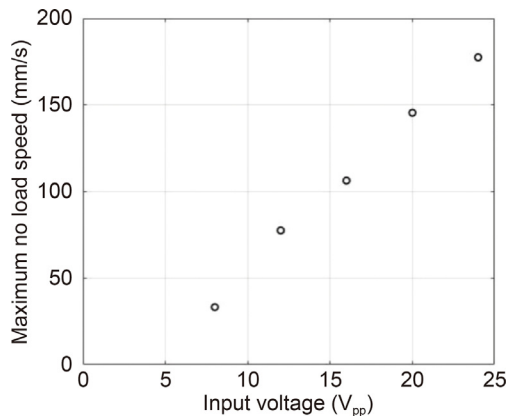


Fig. 11. Maximum NLS results for prototype swimmer in water for various input voltages.

excellent ZSP characteristics. ZSP force per unit area was  $0.83 \text{ mN/mm}^2$ . Even though the measured ZSP result was less than  $0.1 \text{ mN}$  at 96.13 MHz, the swimmer movements and NLS results were recorded and analyzed. At  $24 V_{pp}$ , the NLS result swimmer increased to a maximum of 177 mm/s. The fully submerged SAW propulsion system with high frequency can be more suitable as a small-scale and high-power propulsion system. In future, the effects of fluid resistance and wire traction can be optimized with the overall structure design and wireless system for suitable applications. Because of miniaturization, high power density, and simple structure, the SAW propulsion system with IDTs can be expected for some microrobot applications, such as underwater drone, pipeline robot and intravascular robot.

## Declaration of competing interest

The authors declare that they have no known competing financial interests or personal relationships that could have appeared to influence the work reported in this paper.

## Acknowledgments

This work is based on results obtained from a project, JPNP20004, subsidized by the New Energy and Industrial Technology Development Organization (NEDO).

## References

- [1] C.A. Aubin, S. Choudhury, R. Jerch, L.A. Archer, J.H. Pikul, R.F. Shepherd, Electrolytic vascular systems for energy-dense robots, *Nature* 571 (2019) 51–57.
- [2] L. Paull, S. Saeedi, M. Seto, H. Li, AUV navigation and localization: A review, *IEEE J. Ocean. Eng.* 39 (2013) 131–149.
- [3] T. Huang, H. Gu, B. Nelson, Increasingly intelligent micromachines, *Ann. Rev. Control Robotics Auton Syst* 5 (2022) 279–310.
- [4] B.J. Nelson, I.K. Kaliakatsos, J.J. Abbott, Microrobots for minimally invasive medicine, *Anna. Rev. Biomed. Eng.* 12 (2010) 55–85.
- [5] L. Zhang, J.J. Abbott, L. Dong, B.E. Kratochvil, D.J. Bell, B.J. Nelson, Artificial bacterial flagella: fabrication and magnetic control, *Appl. Phys. Lett.* 94 (2009) 064107.
- [6] D. Ahmed, C. Dillinger, A. Hong, B.J. Nelson, Artificial acousto-magnetic soft microswimmers, *Int. J. Adv. Mater. Technol.* 2 (2017) 1700050.
- [7] C. Zhang, J. Chen, J. Li, Y. Peng, Z. Mao, Large language models for human–robot interaction: A review, *Biomim. Intell. Robotics* (2023) 100131.
- [8] Z. Mao, T. Iizuka, S. Maeda, Bidirectional electrohydrodynamic pump with high symmetrical performance and its application to a tube actuator, *Sensors Actuators A* 332 (2021) 113168.
- [9] H. Gu, Q. Boehler, H. Cui, E. Secchi, G. Savorana, C. Marco, S. Gervasoni, Magnetic cilia carpets with programmable meta-chronal waves, *Nature Commun.* 11 (1) (2022) 1–10.
- [10] T. Huang, H. Huang, D. Jin, Q. Chen, J. Huang, L. Zhang, H. Duan, Four-dimensional micro-building blocks, *Sci. Adv.* 6 (3) (2020) eaav8219.
- [11] H. Gu, Q. Boehler, D. Ahmed, B. Nelson, Magnetic quadrupole assemblies with arbitrary shapes and magnetizations, *Science Robotics* 4 (35) (2019) eaax8977.
- [12] B. Özkale, R. Parreira, A. Bekdemir, L. Pancaldi, E. Özelc, C. Amadio, M. Kaynak, F. Stellacci, D.J. Mooney, M.S. Sakar, Modular soft robotic microdevices for dexterous biomanipulation, *Lab. Chip* 19 (2019) 778–788.
- [13] M. Guix, C.C. Mayorga-Martinez, A. Merckoci, Nano/micromotors in (bio)chemical science application, *Chem. Rev.* 114 (2014) 6285–6322.
- [14] C.R. Knick, D.J. Sharar, A.A. Wilson, G.L. Smith, C.J. Morris, H.A. Bruck, High frequency, low power, electrically actuated shape memory alloy MEMS bimorph thermal actuators, *J. Micromech. Microeng.* 29 (2019) 075005.
- [15] B. Wang, Y. Zhang, L. Zhang, Recent progress on micro-and nano-robots: Towards in vivo tracking and localization, *Quant. Imaging Med. Surg.* 8 (2018) 461.
- [16] D. Mozaffarian, E.J. Benjamin, A.S. Go, D.K. Arnett, M.J. Blaha, M. Cushman, S.R. Das, S. de Ferranti, J.-P. Després, H.J. Fullerton, Heart disease and stroke statistics—2016 update: A report from the American Heart Association, *Circulation* 133 (2016) e38–e360.
- [17] H. Lu, R. Bekker, M. Grundeken, P. Woudstra, J. Wykrzykowska, J. Tijssen, R. de Winter, K. Koch, Five-year clinical follow-up of the STENTYS self-apposing stent in complex coronary anatomy: A single-centre experience with report of specific angiographic indications, *Neth. Heart J.* 26 (2018) 263–271.
- [18] E.M. Purcell, Life at low Reynolds number, *Amer. J. Phys.* 45 (1977) 3–11.

- [19] K. Lee, H. Shao, R. Weissleder, H. Lee, Acoustic purification of extracellular microvesicles, *ACS Nano* 9 (2015) 2321–2327.
- [20] F. Li, X. Xia, Z. Deng, J. Lei, Y. Shen, Q. Lin, W. Zhou, L. Meng, J. Wu, F. Cai, H. Zheng, Ultrafast Rayleigh-like streaming in a sub-wavelength slit between two phononic crystal plates, *J. Appl. Phys.* 125 (2019) 134903.
- [21] F. Li, F. Yan, Z. Chen, J. Lei, J. Yu, M. Chen, W. Zhou, L. Meng, L. Niu, J. Wu, J. Li, F. Cai, H. Zheng, Phononic crystal-enhanced near-boundary streaming for sonoporation, *Appl. Phys. Lett.* 113 (2018) 083701.
- [22] L. Huang, F. Li, F. Cai, L. Meng, W. Zhou, D. Kong, H. Zheng, Phononic crystal-induced standing lamb wave for the translation of subwavelength microparticles, *Appl. Phys. Lett.* 121 (2022) 023505.
- [23] J. Friend, L. Yeo, Encyclopedia of micro- and nanofluidics, in: Chap. Piezoelectric Microdispensers, Springer, New York, 2008, pp. 1662–1672.
- [24] J. Friend, L. Yeo, Microscale acoustofluidics: microfluidics driven via acoustics and ultrasonics, *Rev. Modern Phys.* 83 (2011).
- [25] H. Yun, D. Kong, M. Aoyagi, Characteristics of thickness-vibration-mode PZT transducer for acoustic micropumps, *Sensors Actuators A* 332 (2021) 113206.
- [26] L. Yeo, J. Friend, Ultrafast microfluidics using surface acoustic waves, *Biomicrofluidics* 3 (2009) 012002.
- [27] L. Huang, S. Bao, F. Cai, L. Meng, W. Zhou, J. Zhou, D. Kong, F. Li, H. Zheng, Acoustic rotation of multiple subwavelength cylinders for three-dimensional topography reconstruction, *J. Appl. Phys.* 134 (2023) 20.
- [28] D. Kong, Y. Wang, T. Tsubata, M.K. Kurosawa, M. Aoyagi, Atomization characteristics of 9.6 MHz directional surface acoustic wave for 1-micron spray system, *Sensors Actuators A* 365 (2024) 114911.
- [29] R. Tanimura, D. Kong, M. Aoyagi, Multi-degrees-of-freedom swimmer using an ultrasonic longitudinal transducer, *Japan. J. Appl. Phys.* 61 (2022) SG1038.
- [30] D. Kong, T. Hirata, Y. Wang, F. Li, M.K. Kurosawa, M. Aoyagi, Acoustic underwater propulsion system based on ultrasonic disc PZT transducer, *Sensors Actuators A* 359 (2023) 114502.
- [31] K. Li, X. Zhou, Y. Liu, J. Sun, X. Tian, H. Zheng, L. Zhang, J. Deng, J. Liu, W. Chen, J. Zhao, A 5 cm-scale piezoelectric jetting agile underwater robot, *Adv. Intell. Syst.* (2023) 2200262.
- [32] J. Liu, X. Wang, H. Yu, L. Wang, S. Chen, A small-scale swimmer actuated by acoustic radiation force, *Smart Mater. Struct.* 32 (2023) 115002.
- [33] D. Kong, T. Hirata, Y. Wang, F. Li, M.K. Kurosawa, M. Aoyagi, A novel miniature swimmer propelled by 36° Y-cut lithium niobate acoustic propulsion system, *Sensors Actuators A* 365 (2024) 114837.
- [34] Y. Bourquin, J.M. Cooper, Swimming using surface acoustic waves, *PLoS One* 8 (2013) e42686.
- [35] D. Kong, K. Nishio, M.K. Kurosawa, Surface acoustic wave propulsion system with acoustic radiation force, *Sensors Actuators A Phys.* 309 (2020) 111943.
- [36] N. Zhang, Y. Wen, J. Friend, MHz-order surface acoustic wave thruster for underwater silent propulsion, *micromachines* (2020) 11419.
- [37] D. Kong, R. Tanimura, F. Wang, K. Zhang, M.K. Kurosawa, M. Aoyagi, Submerged surface acoustic wave propulsion system with SiO<sub>2</sub>/Al/LN structure, in: Proc, IEEE Ultrasonics Symp, 2023, pp. 1–2.
- [38] W.L. Nyborg, Acoustic Streaming Physical Acoustics, Principles and Methods, vol. 2, Part B, Academic Press, 1965, pp. 265–331.
- [39] J. Lighthill, Acoustic streaming, *J. Sound Vib.* 61 (1978) 391–418.
- [40] S. Shiokawa, Y. Matsui, T. Moriizumi, Experimental study on liquid streaming by SAW, *Japan. J. Appl. Phys.* 28 (1989) 126–128.
- [41] A.A.S. Junior, Ultrasonic Waves, vol. 147, 2012.
- [42] J. Wu, J. Niu, Y. Liu, X. Rong, R. Song, H. Dong, J. Zhao, Y. Li, Development of a self-moving ultrasonic actuator with high carrying/towing capability driven by longitudinal traveling wave, *IEEE/ASME Trans. Mechatron.* 28 (1) (2023) 267–279.
- [43] J. Wu, L. Wang, F. Du, G. Zhang, J. Niu, X. Rong, R. Song, H. Dong, J. Zhao, Y. Li, A two-DOF linear ultrasonic motor utilizing the actuating approach of longitudinal-traveling-wave/bending-standing-wave hybrid excitation, *Inter. J. Mech. Sci.* 248 (2023) 108223.
- [44] M.K. Kurosawa, State-of-art surface acoustic wave linear motor and its future applications, *Ultrasonics* 38 (2000) 15–19.
- [45] T. Shigematsu, M.K. Kurosawa, Miniaturized SAW motor with 100 MHz drive frequency, *IEEE Trans. Sens. Micromach.* 126 (2006) 166–167.
- [46] Y. Kurokawa, H. Taki, S. Yashiro, K. Nagasawa, Y. Ishigaki, H. Kanai, Estimation of size of red blood cell aggregates using backscattering property of high-frequency ultrasound: in vivo evaluation, *J. Appl. Phys.* 55 (1–8) (2016) 07KF12.
- [47] A. Sano, Y. Matsui, S. Shiokawa, New manipulator based on surface acoustic wave streaming, *Japan. J. Appl. Phys.* 37 (1998) 2979–2981.